

# Physical and Electrochemical Properties of LiFePO<sub>4</sub>/C Composite Cathode Prepared From Aromatic Diketone-Containing Precursors

Hong-Chang Wong, James R. Carey, Jenn-Shing Chen\*

Department of Applied Chemistry, National University of Kaohsiung, Kaohsiung City, Taiwan 811, R.O.C.

\*E-Mail: [jschen@nuk.edu.tw](mailto:jschen@nuk.edu.tw)

Received: 30 June 2010 / Accepted: 15 July 2010 / Published: 10 August 2010

---

A systematic study of the relationship between the carbon precursor structure and the discharge capacity in LiFePO<sub>4</sub>/C composite materials is presented. Knowledge of this relationship may yield composites with improved electrochemical and tailor made properties. To this end, we describe the effects of organic additives with functionalized aromatic diketones on the performance of a LiFePO<sub>4</sub>/C composite cathode. Described herein, is a coprecipitation method resulting in a series of LiFePO<sub>4</sub>/C materials by calcinating amorphous LiFePO<sub>4</sub> with various structures of diketone additives at 700°C. X-ray diffraction, scanning electron microscopy (SEM), particle size analysis (PSA), thermal analysis, Raman spectral analysis, BET surface area and electrochemical data indicate that aromatic diketones with increasing length of alkoxy chains possess improved capacities compared to other various types of organic reagents. This finding may pave the way for new LiFePO<sub>4</sub> materials with enhanced electrochemical properties.

---

**Keywords:** Lithium iron phosphate, carbon coating, cathode material, coprecipitation

## 1. INTRODUCTION

In recent years, olivine-type cathode materials of LiFePO<sub>4</sub> have been extensively studied for use in Li-ion batteries because of its high theoretical capacity (170 mAh g<sup>-1</sup>), good cycling stability, low cost, and environmental friendliness. These attractive characteristics make olivine LiFePO<sub>4</sub> a good candidate for use in large scale Li-ion batteries for electric vehicle (EV) and hybrid electric vehicle (HEV) applications. Despite these favorable characteristics, their widespread use is hampered by its

poor rate performance. The salient feature responsible for its poor rate capability is thought to be its intrinsically poor electronic conductivity (of the order of  $10^{-9}$  S cm<sup>-2</sup>) [1-3].

In order to increase the electronic conductivity of these composites, several strategies have been adopted such as optimization of synthetic procedures [4-6], carbon nanocoating [7,8], particle-size minimization [9], metal powder addition [10,11], doping with supervalent ions [12,13], and carbothermal formation of the surface conducting phase [12-16]. To date, the majority of these studies have focused on the incorporation of conductive carbon into active material powders to form carbon-coated LiFePO<sub>4</sub> (LiFePO<sub>4</sub>/C) composites. The behavior of these LiFePO<sub>4</sub>/C composites is related to the phase purity of the active material, particle size, structure of the carbon additive, the carbon content, form of carbon contact, and the mixing and sintering recipe.

Recently, the relationship of the performance of the LiFePO<sub>4</sub>/C composites to the carbon structural parameters derived from Raman analysis has been investigated [15-20]. The results indicate that the selected carbon precursors directly affected the characteristics of the carbon additive, which in turn is related to the performance of the LiFePO<sub>4</sub>/C composite. In addition, it has been demonstrated elsewhere that the selection of organic precursor as a carbon source is very important for tailoring the final properties of carbon coated composite powders [3-16, 18]. It was found that more highly graphitized carbons are formed during pyrolysis when using functionalized aromatic or ring-forming reagents [14-17].

According to our earlier studies, aromatic diketones with alkoxy chains with increasing length (at the meta and para position to the diketone) produced LiFePO<sub>4</sub> composites with improved electrochemical performances [18]. Taken together, the data suggest that the improved discharge capacities are due to high carbon content, small particle sizes, and uniformly coated layers that contain optimized ratios of sp<sup>2</sup>/sp<sup>3</sup> bond character. It is clear that the performance controlling factors are strongly related the type, amount and heat treatment of the carbon precursors. Based on these results, we selected additional organic motifs with functionalized aromatic diketones as carbon precursors to determine the nature of the precursor to the properties of the LiFePO<sub>4</sub>/C composite.

Due to the inherent complexity of these systems, we set out to investigate and fine tune the aforementioned performance controlling properties by studying several of structural motifs. These structural motifs were selected in an attempt to converge a unified theory of how to improve performance properties with these important LiFePO<sub>4</sub> composites. Four separate structural motifs were selected: 1(a-c)(alkoxy chains with increasing length at the meta and para position), 2 (fused rings with heteroatoms), 3 (fused diketone rings with long alkoxy chains at the meta and para position to the diketone), and 4 (fused diketone rings with no alkoxy chains). Relative amounts of the carbon precursors with LiFePO<sub>4</sub> were also varied and thoroughly investigated.

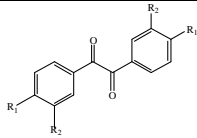
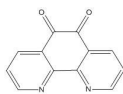
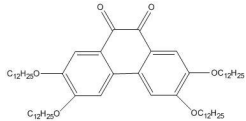
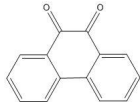
A coprecipitation method was adopted to prepare LiFePO<sub>4</sub> and its carbon composites because of its simplicity and low cost [18]. Moreover; it is simple to control the amount and characteristics of residual carbon on the surface of the LiFePO<sub>4</sub> particles from the various sources of organic reagents. In order to obtain a uniform carbon distribution, an *in-situ* coating of carbon on the LiFePO<sub>4</sub> was performed by the pyrolysis of the organic additives. The organic additives were first dissolved in an appropriate solvent and then homogeneously mixed with amorphous LiFePO<sub>4</sub> particles before the final heating step. A series of residual carbons on the surface of prepared LiFePO<sub>4</sub> materials originating

from the pyrolysis of different organic reagents were characterized. The electrochemical properties of as-prepared  $\text{LiFePO}_4/\text{C}$  composites as cathodes in Li-ion cells were measured from cyclic voltammogram (CV) and charge-discharge tests.

## 2. EXPERIMENTAL PART

$\text{LiFePO}_4$  and its carbon composites were prepared by a co-precipitation method in de-ionized water at room temperature. The modified method of Prosini *et al.* [18,19] was applied to synthesize the  $\text{LiFePO}_4/\text{C}$  composites. Amorphous  $\text{LiFePO}_4$  was obtained by the chemical lithiation of amorphous  $\text{FePO}_4$  using Li as a reducing agent [18]. The solutions of carbon additive precursors prepared by dissolving the various organic reagents selected solvents are listed in Table 1. Organic solutions were mixed with amorphous  $\text{LiFePO}_4$  particles and the solution was heat-treated in a tubular furnace at  $750^\circ\text{C}$  for 8 h under reducing atmosphere ( $\text{Ar}/\text{H}_2 = 95/5$ ).

**Table 1.**  $\text{LiFePO}_4$  samples processed with organic additives.

Compound	Structure	Solvent
1(a-c)	 <p>1a : <math>\text{R}_1=\text{R}_2=\text{OC}_6\text{H}_{13}</math>            1b : <math>\text{R}_1=\text{R}_2=\text{OC}_{10}\text{H}_{21}</math>            1c : <math>\text{R}_1=\text{R}_2=\text{OC}_{12}\text{H}_{25}</math></p>	Dichloro methane
2 (1,10-Phenanthroline-5,6-dione)		Acetone
3 (2,3,6,7-tetradodecyloxy-phenanthrene-9,10-diones)		Acetone
4 (9,10-phenanthrenequinone)		Acetone

A Rigaku-D/MaX-2550 diffractometer with Cu  $K_\alpha$  radiation ( $\lambda=1.54 \text{ \AA}$ ) was used to obtain X-ray diffraction (XRD) patterns for the samples. The morphology of the sample was observed by a

scanning electron microscope (SEM, Hitachi S-4300) and transmission electron microscope (TEM, JEOL JEM-2010). Particle size analysis (PSA) was carried out with a Malvern particle size analyzer (Zetasizer Nano ZS). An integrated Raman microscope system (JOBIN-YVON T64000) was used to analyze the structure and composition of the individual particles in  $\text{LiFePO}_4$ . Thermogravimetry (TG) apparatus (SETARAM) was used for the thermal analysis. The specific surface area was measured by using a Brunauer-Emmett-Teller (BET) apparatus (ASAP2020). The residual carbon content of the powders was determined by means of an automatic elemental analyzer (Elementar vario, EL III).

For electrochemical evaluation, the composite electrodes were prepared by wet coating, and were made from as-prepared  $\text{LiFePO}_4/\text{C}$  with acetylene black, SFG-6 synthetic flake graphite (Timcal Ltd.), and polyvinylidene fluoride (PVDF) binder (MKB-212C, Elf Atochem) in a weight ratio of 80:5:5:10. The  $\text{LiFePO}_4/\text{C}$  active materials, acetylene black and SFG-6 were first added to a solution of PVDF in *n*-methyl-2-pyrrolidone (NMP, Riedel-deHaen). The mixture is stirred for 20 min at room temperature using a magnetic stir bar, and then with a turbine for 5 min at 2000 rpm to produce a slurry with an appropriate viscosity. The resulting slurry was coated onto a piece of Al foil and dried at 120°C for 40 min. The coating was ~100  $\mu\text{m}$  thick with an active material mass loading of  $8 \pm 1 \text{ mg cm}^{-2}$ . The quantity of active materials on the electrodes was kept constant. Electrodes were dried overnight at 100°C under vacuum before being transferred to an argon-filled glove box for cell assembly. Electrodes were placed in an open glass bottle cell with a 1  $\text{cm}^2$  square  $\text{LiFePO}_4/\text{C}$  cathode electrode and Li foil as the counter and reference electrodes for CV experiments. Coin cells of 2032 size were assembled using Li metal as a counter electrode. In all cells, a solution of 1 M  $\text{LiPF}_6$  in a mixed solvent of ethylene carbonate/dimethyl carbonate (EC/DMC) with 1:1 volume ratio was used as the electrolyte. CV experiments were carried out using a CHI 704A potentiostat at variable scan rates from 1 to 0.01  $\text{mV s}^{-1}$ . Coin cells were cycled galvanostatically with a BAT-750B (Acu Tech System) at a constant current of 0.5C with a voltage region of 2.5 – 4.2 V vs  $\text{Li}/\text{Li}^+$  at room temperature; (1C equals 170  $\text{mA g}^{-1}$ ). The current density was calculated based on the mass of  $\text{LiFePO}_4/\text{C}$  contained in the electrode.

### 3. RESULTS AND DISCUSSIONS

The carbon-coated  $\text{LiFePO}_4$  ( $\text{LiFePO}_4/\text{C}$ ) electrode was investigated in this study due its improved conductivity relative to  $\text{LiFePO}_4$  without carbon. Recent studies [15-16,18,20] have reported that the organic additives pyrolysis method is a relatively simple method for coating fine particles via a carbon layer, and the structure of the pyrolyzed reagents directly affect the final quality of carbon-coated composite powders. To determine the nature of this phenomenon, we investigated several of organic precursor structural motifs and determined their relationship to the electrochemical performance and the physical properties of the resulting  $\text{LiFePO}_4/\text{C}$  composites.

Four distinct types of organic reagents, 1-4, were studied to assess their effects as additives. The structures of organic reagents and their solvents are listed in Table 1. Here, we adopted 1 as the control sample for comparison purposes since it has performed well according to our earlier studies [18]. All prepared  $\text{LiFePO}_4/\text{C}$  powders were deep black in color, in contrast to the gray color of pure

LiFePO<sub>4</sub> powders. Figure 1 shows the XRD patterns of the prepared samples. The XRD pattern of LiFePO<sub>4</sub> without carbon (Figure 1b) showed a single phase with an ordered olivine structure indexed to the orthorhombic *Pnmb* space group (Figure 1a).

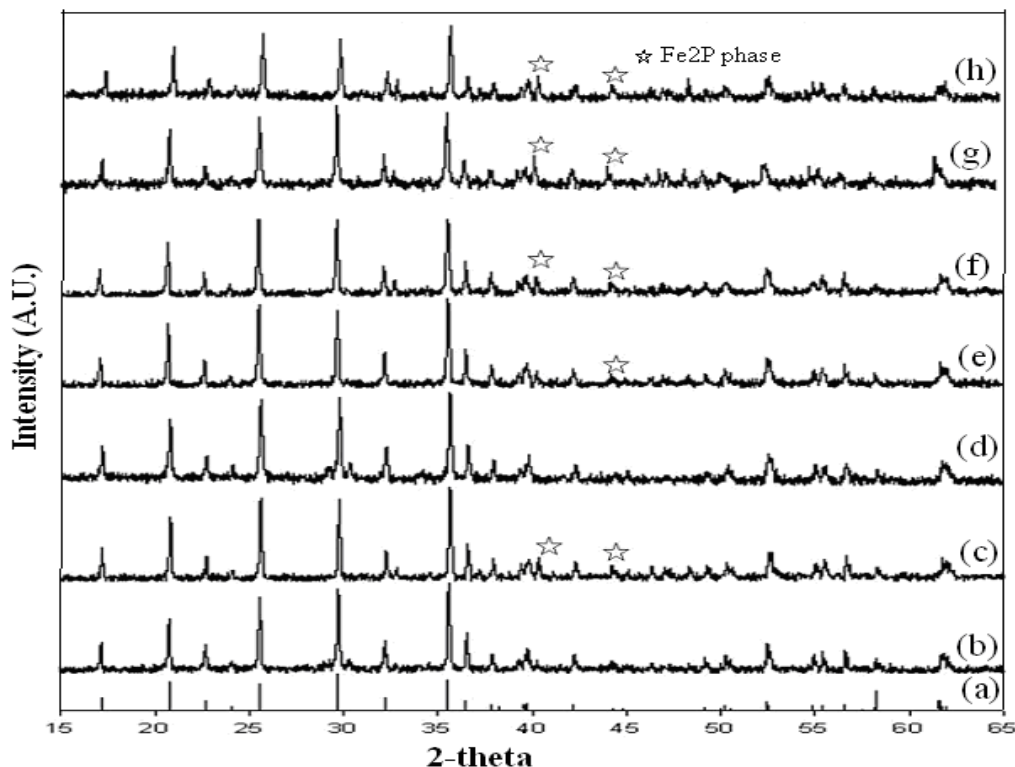


**Figure 1.** XRD patterns of (a) theoretical pattern, (b) pure LiFePO<sub>4</sub>, (c) 4, (d) 2, (e) 3, (f) 1a, (g) 1b, (h) 1c.

Xu *et al.* [21] have shown that Fe<sub>2</sub>P has an electronic conductivity of about 1.5 S cm<sup>-1</sup> and the existence of the impure Fe<sub>2</sub>P phase in LiFePO<sub>4</sub>/C materials plays an important role for improving the electronic-conductivity and electrochemical performance of LiFePO<sub>4</sub>/C materials, such as less polarization phenomenon, high reversible capability and decreased loss of rate capability. Indeed, a minor impurity phase exists in our samples that can be indexed to Fe<sub>2</sub>P (Figs. 1c-h). Major changes are not observed in the olivine XRD pattern, indicating that the olivine-type structure is maintained when using additives 1-4. According to our earlier studies [18], the Fe<sub>2</sub>P phase is evident for LiFePO<sub>4</sub>/C composites heated above 675°C. In addition, several reports [2,14-15,21-22] have concluded that high temperatures or an increase in carbon content can enhance the reducing ability of carbon such that the Fe and P are reduced to form inactive Fe<sub>2</sub>P.

Various organic reagents were thermally analyzed in order to examine the effect of their thermal decomposition on the behavior of the composites. The TG curves of all powder mixtures consisting of amorphous LiFePO<sub>4</sub> with various organic reagents are shown in Figure 2. As shown in the TG curves in Figure 3, all organic reagents exhibit appreciable, rapid, weight-loss over a

temperature range that corresponds to pyrolysis and decomposition. In addition, a small gradual weight loss continues until 700°C, and is thought to be the pyrolysis of the remaining organics.

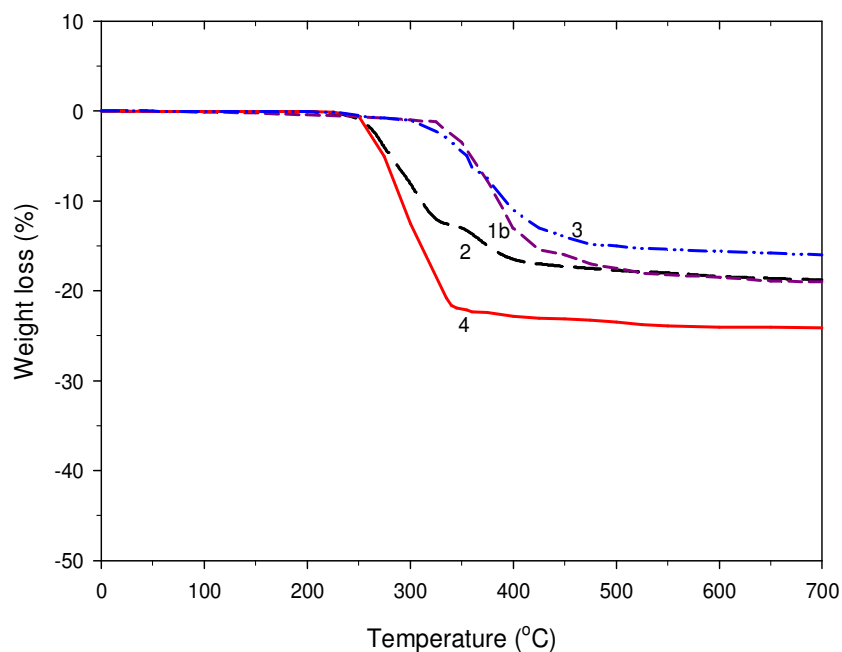


**Figure 2.** TGA of various organic reagents measured at a heating rate of  $5^{\circ}\text{C}\cdot\text{min}^{-1}$  in nitrogen at a  $60\text{ mL}\cdot\text{min}^{-1}$  flow rate.

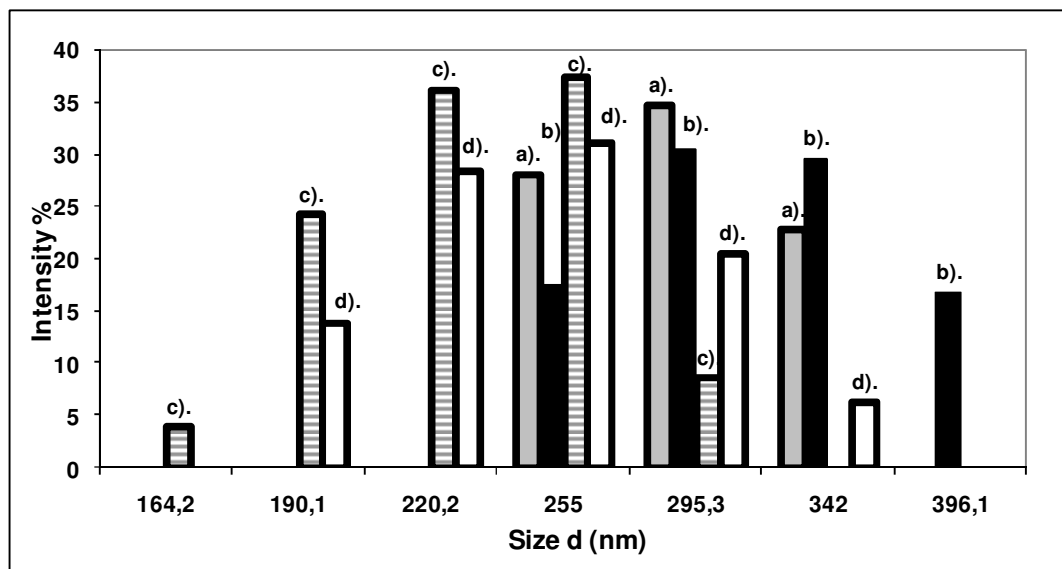


**Figure 3.** Particle size distribution for a  $\text{LiFePO}_4/\text{C}$  composites containing (a) 4 ( $Z_{\text{avg}}=349.3$ ;  $\text{PDI}=0.210$ ), (b) 2 ( $Z_{\text{avg}}=322.9$ ;  $\text{PDI}=0.262$ ), (c) 1b ( $Z_{\text{avg}}=234.1$ ;  $\text{PDI}=0.170$ ), (d) 3 ( $Z_{\text{avg}}=241.9$ ;  $\text{PDI}=0.113$ ).

This indicates that the organic reagents are pyrolyzed rather than evaporated during successive thermal treatments. The final quantity of residual carbon (~0.8-1.4 wt%) for the pyrolysis of the organic reagents was measured using an elemental analyzer (EA). Table 2 presents the decomposition temperature range, residual carbon content and BET surface area for various organic reagents. Together, these data strongly suggest that the differences in the structures of organic reagents affect the

**Table 2.** Comparison of the decomposition temperature, weight loss at 800°C and BET

Sample	Decomposed Temperature ( °C )	Residual carbon content (wt%)	BET surface area (m <sup>2</sup> g <sup>-1</sup> )
1a	390-430	1.25	12.56
1b	400-470	1.41	13.42
1c	410-475	1.46	14.42
2	275-400	1.03	9.34
3	330-430	1.35	11.02
4	275-320	0.82	2.52

decomposition temperature range.

Indeed, the transformation temperature from an amorphous to a crystalline phase of a LiFePO<sub>4</sub> composite has been studied at ~470°C [23-25]. There is an obvious correlation between the electrochemical capacity of LiFePO<sub>4</sub>/C composites and the temperature difference between the decomposition of organic reagents and the phase transformation of LiFePO<sub>4</sub> [18,23]. As mentioned in our previous study [18,20], while the temperature difference is small, a synchronous process of LiFePO<sub>4</sub> crystallization and organic reagent pyrolysis occurs similar to an *in situ* synthesis of the LiFePO<sub>4</sub>/C composite. The highly active carbon, generated from pyrolysis, homogeneously coats carbon on the surface of freshly crystallized LiFePO<sub>4</sub> particles. This homogenous coating efficiently hinders particle growth causing the formation of a composite possessing a fine particle size and a surface with uniform carbon distribution.

The TG curves illustrate that the decomposition temperature of 1b is close to the temperature of the LiFePO<sub>4</sub> phase transformation. As shown in Table 2, 1(a-c) outperformed all other organic reagents in this study because the decomposition temperatures are close to the temperature of the LiFePO<sub>4</sub> phase transformation. Figure 3 shows the mean particle size of 4, 2, 1b and 3, respectively. 1b and 3 have smaller particle sizes resulting in larger surface areas. Figure 4 shows the SEM images of LiFePO<sub>4</sub>/C composites containing 1b. 1b displays a rather homogeneous and smaller particle distribution. The average particle size was ~200 nm, which is in good agreement with the measurement from PSA (Figure 3c). In addition, the BET analysis gives a specific surface area of about 11.02,

12.56, 13.42 and 14.42  $\text{m}^2\cdot\text{g}^{-1}$  for the crystalline material of the 3, 1a, 1b, and 1c, respectively. In summary, 1b and 1c have smaller particle sizes resulting in larger surface areas.

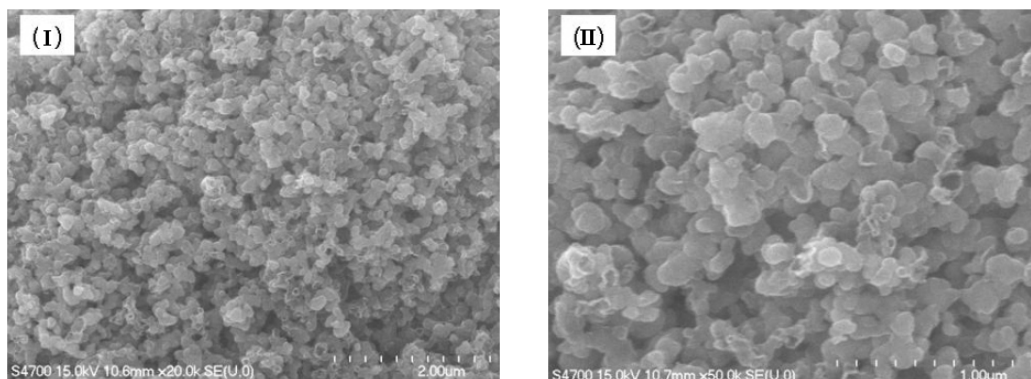


**Figure 4.** Scanning electron microscopy (SEM) images of  $\text{LiFePO}_4/\text{C}$  composite cathode materials containing 1b (I and II) at low and high magnifications, respectively.

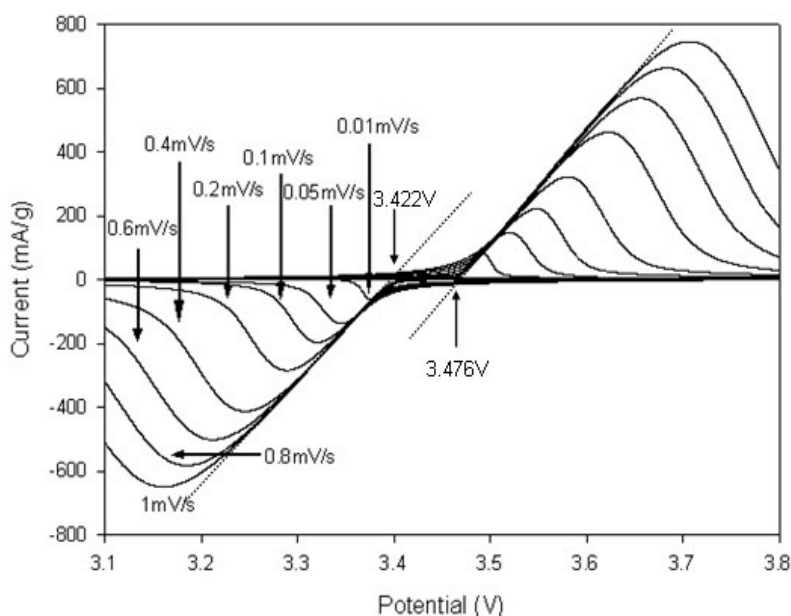


**Figure 5.** Cyclic voltammograms profiles of  $\text{LiFePO}_4/\text{C}$  using 1b at different scan rate. (dashed lines are the extrapolations of the initial current potential lines to the x axis).

$\text{LiFePO}_4/\text{C}$  electrodes were studied in a beaker cell which was cycled between 3.0 and 4.0 V with various scan rates between 0.01-1.0  $\text{mV s}^{-1}$ , using a 1 M  $\text{LiBF}_4 + \text{EC}/\text{DMC}$  (1:1) electrolyte. Figure 5 shows the CV curves of  $\text{LiFePO}_4/\text{C}$  with 1b at various scan rates, and the peak separation increases with scan rate. All CV profiles overlap regardless of scan rate at the beginning of charging and discharging. In theory, if a reversible reaction corresponds to an extremely small scan rate, the true separation between the anodic and cathodic peaks is 58 mV at 25°C [26]. In practice, the lowest scan



rate of  $0.01 \text{ mV s}^{-1}$  is the limit of the test equipment. The CV profiles overlap each other initially; we can circumvent this limitation by extrapolating the envelope of the CV profiles to the x axis to obtain the anodic and cathodic potential for a reversible reaction. Extrapolations of the initial current, shown in Figure 5 as dashed lines, yields anodic and cathodic potentials of 3.476 V and 3.422 V respectively. The potential difference of CV profiles in 1b is roughly 54 mV as shown in Figure 5, which is within the limit of 58 mV at  $25^\circ\text{C}$ , indicating a reversible redox process for Li ion reactions.

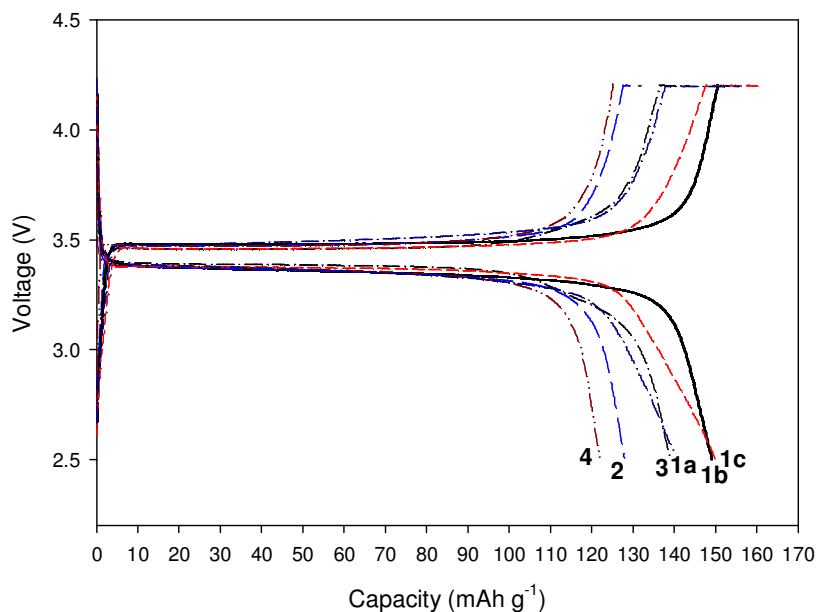
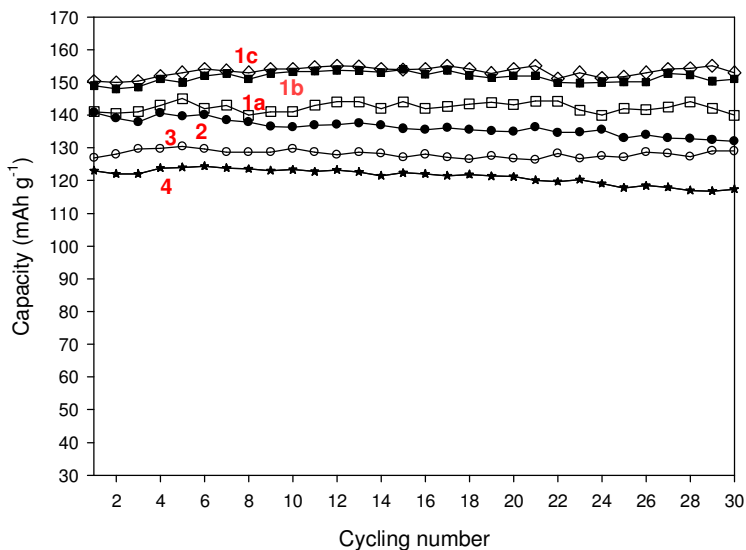


**Figure 6.** Voltage profiles of Li/LiFePO<sub>4</sub> cells containing various organic additives recorded during the second cycle at 0.5C rate between 2.5 and 4.2 V.

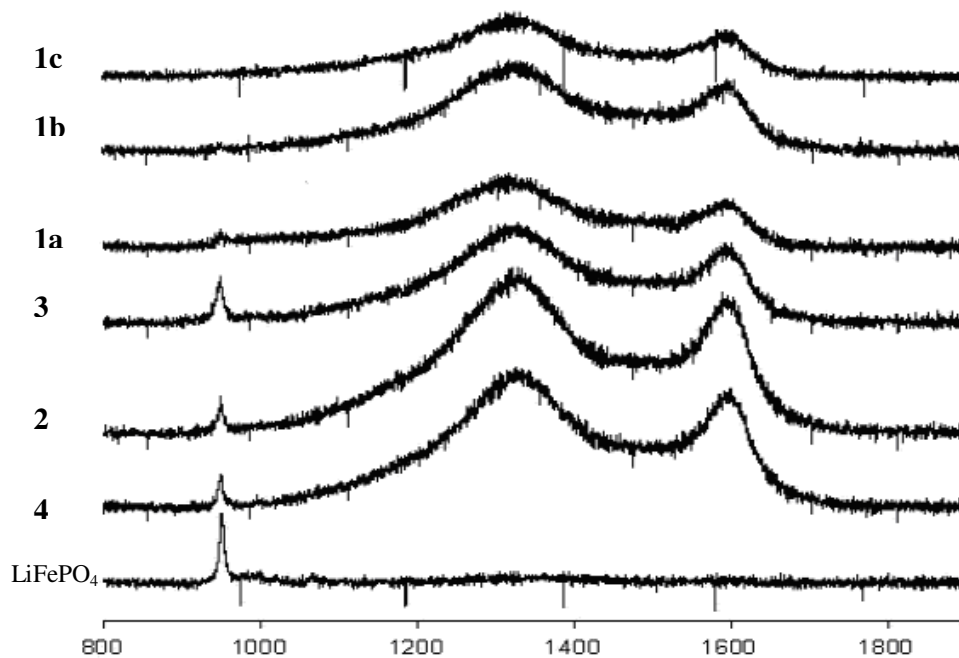
Figure 6 shows the charge-discharge voltage profiles of Li/LiFePO<sub>4</sub> cells containing different organic additives at a 0.5C rate between 2.5 and 4.2 V during the second cycle. A charge-discharge curve plateau over a wide voltage range at approximately 3.4 V (versus Li/Li<sup>+</sup>) implies that a two-phase Fe<sup>3+</sup>/Fe<sup>2+</sup> redox reaction proceeds via a first-order transition between FePO<sub>4</sub> and LiFePO<sub>4</sub>. The small voltage difference between the charge-discharge plateaus indicates good kinetics. As shown in Figure 6, 1c (150 mAh g<sup>-1</sup>) and 1b (149 mAh g<sup>-1</sup>) contain longer alkoxy branches and deliver a larger discharge capacity during the second cycle. In contrast, 4 delivers the smallest charge capacity at 125 mAh g<sup>-1</sup> during the second cycle and discharge capacity of 122 mAh g<sup>-1</sup>.

Figure 7 shows a plot of capacity versus cycle number for Li/LiFePO<sub>4</sub> cells containing different organic additives at 0.5C rate. The coulombic efficiency of all samples is at least 97%, which is in good agreement with the CV measurements. All cells display good capacity retention after 30 cycles. The cell discharge capacity displays a strong relationship between the type of additive and decomposition temperature. 1b and 1c have a similar capacity owing to the similarity of their decomposition temperature curves. Both 1b and 1c outperformed all other reagents because their

decomposition temperatures are close to the temperature of the  $\text{LiFePO}_4$  phase transformation, which causes the formation of a composite with a fine particle size and uniform surface carbon distribution. Composites made with 4 display a lower decomposition temperature, higher weight loss and subsequently yield a lower capacity.



**Figure 7.** Discharge capacity vs. cycle number at 0.5C rate between 2.5 and 4.2 V for  $\text{Li/LiFePO}_4$  cells containing different organic additives.



**Figure 8.** Raman spectra of  $\text{LiFePO}_4$  and  $\text{LiFePO}_4/\text{C}$  powders.

The structure of the deposited carbon was investigated by Raman spectroscopy. Figure 8 displays the Raman spectra of the  $\text{LiFePO}_4$  and  $\text{LiFePO}_4/\text{C}$  composites with made with 4, 2, 3, 1a, 1b, and 1c respectively. All spectra consisted of a small band at  $940\text{ cm}^{-1}$  corresponding to the symmetric  $\text{PO}_4$  stretching model of  $\text{LiFePO}_4$ . Two intense broad bands at  $1350$  and  $1585\text{ cm}^{-1}$  can be assigned to the D and G bands of residual carbon in the  $\text{LiFePO}_4/\text{C}$  composite, respectively. The spectrum of pure  $\text{LiFePO}_4$  does not possess D and G bands, which represent the absence of carbon on the surface. Thus, the difference in discharge capacity may be caused by the effect of the structure of the organic additives on the characteristic of the surface carbon on the  $\text{LiFePO}_4/\text{C}$  composite.

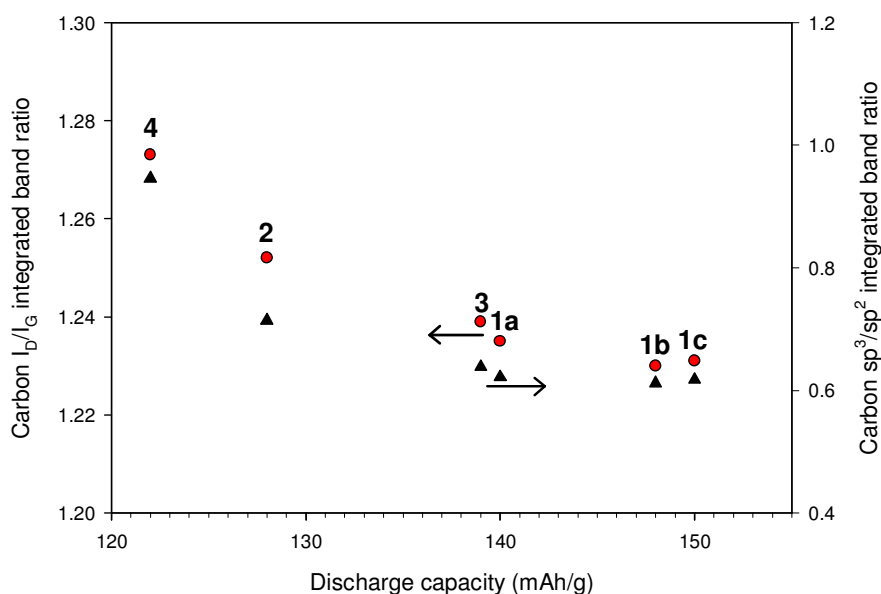


**Figure 9.** Relationship of Raman intensity ratio of D/G bands and  $sp^3/sp^2$  coordinated carbon with discharge capacity for various organic additives ( $\bullet$   $I_D/I_G$ ,  $\blacktriangle$   $sp^3/sp^2$ ).

The D and G bands were composed of four signals located at  $1194$ ,  $1347$ ,  $1510$ , and  $1585\text{ cm}^{-1}$  [15-18]. The observed spectra were analyzed by a pseudo-Voigt profile function, and separated numerically into four signals. The bands at  $1347$  and  $1585\text{ cm}^{-1}$  have been assigned to the  $sp^2$  graphite-like structure, whereas all other observed bands are attributed to the  $sp^3$  tetrahedral carbon, which is often observed in highly amorphous carbonaceous materials [16]. The  $sp^3/sp^2$  ratio was estimated to be  $\sim 0.6-0.9$  for all species. This indicates that the fraction of graphite-like carbon was  $\sim 60\%$  and the conducting path was mainly due to graphite-like carbon. In addition, the intensity ratio  $R = I_D/I_G$  defines the level of order and the in-plan crystal size for the pyrolytic carbon. Both  $I_D/I_G$  and  $sp^3/sp^2$  parameters as a function of different organic reagents are shown in Figure 9.

Composites synthesized using 1c yield the lowest  $I_D/I_G$  and  $sp^3/sp^2$  values, but exhibit the highest discharge capacities. In addition, 1b and 1c have similar  $I_D/I_G$  and  $sp^3/sp^2$  values, and exhibit a similar discharge capacity. In general, higher capacities are directly correlated with low values of the  $I_D/I_G$  and  $sp^3/sp^2$  parameters. The low values for the  $I_D/I_G$  and  $sp^3/sp^2$  parameters indicate a high degree

of graphitization. Increasing the degree of graphitization can not only improve the electronic conductivity of residual carbon by providing better electronic contact between submicrometer particles with large agglomerates, but can also yield improved electrode performance [20,27]. The aromatic diketone with a longer alkoxy chains such as 1(a-c) contains a large number of functionalized aromatic and/or conjugated double bond structural motifs. This may influence the formation of more highly graphite-like carbons during pyrolysis yielding composites with better electrochemical performance.

According to our previous investigations [18], the choice of an appropriate carbon precursor is an important factor controlling the performance of the  $\text{LiFePO}_4/\text{C}$  composite and the beneficial effects include (i) increased carbon retention, (ii) production of carbon during a critical stage of the calcination process to limit grain growth and increase homogeneity, and (iii) improvement of the residual carbon structure. In this work, we find that 1(b-c) are suitable for producing a  $\text{LiFePO}_4/\text{C}$  composites with fine particle sizes, and a uniformly coated carbon conductive layer, resulting in improved electrochemical performance. The major beneficial effects for 1(b-c) as an organic additive are that it promotes a synchronous process of  $\text{LiFePO}_4$  crystallization, and an increase in the production of larger graphene clusters in the disordered carbon structure after pyrolysis. In general, the structures of the organic additives with increased functionalization of aromatics and/or conjugate double bond, such as 1(b-c), are suitable for producing  $\text{LiFePO}_4/\text{C}$  composites with fine particle sizes, uniformly coated carbon conductive layers, and improved electrochemical performance.

#### 4. CONCLUSIONS

In this work, four separate organic motifs were selected as carbon additives to study the relationship of precursor structure to the performance of  $\text{LiFePO}_4$  composites. The motifs include: 1(a-c) (alkoxy chains with increasing length at the meta and para position), 2 (fused rings with heteroatoms), 3 (fused diketone rings with long alkoxy chains at the meta and para position to the diketone), and 4 (fused diketone rings with no alkoxy chains). We have illustrated that the choice of an appropriate organic precursor is an important factor controlling the performance of  $\text{LiFePO}_4$  materials. The beneficial effects include: (i) increased carbon retention, (ii) production of carbon during a critical stage of the calcinations process resulting in grain growth limitations and increases in homogeneity, (iii) improvement of the residual carbon structure, and (iv) the possibility of the formation of a more conductive  $\text{Fe}_2\text{P}$  phase. The aromatic diketones 1(b-c) possess an increase in alkoxy chain length and were found to be suitable for the production  $\text{LiFePO}_4/\text{C}$  composites with fine particle sizes, a uniformly coated carbon conductive layer, and improved electrochemical performance. Now that a basic understanding of performance enhancing effects and their relationship to the carbon precursor structure is understood, our future goal will be to find other performance enhancing effects and combine them with the enhancements described in this work.

#### ACKNOWLEDGMENTS

The authors wish to thank the National Science Council of Taiwan for financial support under contract no. NSC-95-2113-M-390-005-MY3. The authors also wish to thank Professor Ong, C. W. for providing the organic materials.

**References**

1. A.K. Padhi, K.S. Nanjundaswamy, J.B. Goodenough, *J. Electrochem. Soc.* 144 (1997) 1188-1194.
2. B.L. Ellis, K. Y. Lee, L.F. Nazar, *Chem. Mater.* 22 (2010) 691-714.
3. K. Striebel, J. Shim, V. Srinivasan, J. Newman, *J. Electrochem. Soc.* 152 (2005) A664-A670.
4. B. Kang, G. Ceder, *Nature* 458 (2009) 190-193.
5. G. Arnold, J. Garche, R. Hemmer, S. Strobele, C. Vogler, M. Wohlfahrt-Mehrens, *J. Power Sources* 119-121 (2003) 247-251.
6. R. Santhanam, B. Rambabu, *Int. J. Electrochem. Sci.*, 4 (2009) 1770-1778.
7. H. Huang, S.C. Yin, L.F. Nazar, *Electrochem. Solid State Lett.* 4 (2001) A170-A172.
8. Z. Chen, J.R. Dahn, *J. Electrochem. Soc.* 149 (2002) A1184-A1189.
9. Yamada, S.C. Chung, K. Hinokuma, *J. Electrochem. Soc.* 148 (2001) A224-A229.
10. F. Croce, A.D. Epifanio, J. Hassoun, A. Deptula, T. Olczac, B. Scrosati, *Electrochem. Solid State Lett.* 5 (2002) 47-50.
11. K.S. Park, J.T. Son, H.T. Chung, S.J. Kim, C.H. Lee, K.T. Kang, H.G. Kim, *Solid State Commun.* 129 (2004) 311-314.
12. S.Y. Chung, J.T. Bloking, Y.M. Chiang, *Nat. Mater.* 1 (2002) 123-128.
13. N. Jayaprakash, N. Kalaiselvi, P. Periasamy, *Int. J. Electrochem. Sci.*, 3 (2008) 476-488.
14. P.S. Herie, B. Ellis, N. Coombs, L.F. Nazar, *Nat. Mater.* 3 (2004) 147-152.
15. M. Doeff, Y. Hu, F. McLarnon, R. Kostecki, *Electrochem. Solid State Lett.* 6 (2003) A207-A209.
16. Y. Hu, M. Doeff, R. Kostecki, R. Finones, *J. Electrochem. Soc.* 151 (2004) A1279-1285.
17. T. Nakamura, Y. Miwa, M. Tabuchi, Y. Yamada, *J. Electrochem. Soc.* 153 (2006) A1108-A1114.
18. C.W. Ong, Y.K. Lin, J.S. Chen, *J. Electrochem. Soc.* 154 (2007) A527-A533.
19. P.P. Prosini, M. Caewwska, S. Suaccia, P. Wisniewski, S. Passerine, M. Pasquali, *J. Electrochem. Soc.* 149 (2002) A886-A890.
20. Y.H. Nien, J.R. Carey, J.S. Chen, *J. Power Sources* 193 (2009) 822-827.
21. Y. Xu, Y. Lu, L. Yan, Z. Yang, R. Yang, *J. Power Sources* 160 (2006) 570-576.
22. C.M. Doherty, R.A. Caruso, B.M. Smarsly, C.J. Drummond, *Chem. Mater.* 21 (2009) 2895-2903.
23. C.H. Mi, X.B. Zhao, G.S. Cao, J.P. Tu, *J. Electrochem. Soc.* 152 (2005) A483-A487.
24. N. Yun, H.W. Ha, K.H. Jeong, H.Y. Park, K. Kim, *J. Power Sources* 160 (2006) 1361-1368.
25. H. Liu, Y. Feng, Z. Wang, K. Wang, J. Xie, *Powder Technology* 184 (2008) 313-317.
26. D.Y.W. Yu, C. Fietzek, W. Weydanz, K. Donoue, T. Inoue, H. Kurokawa, S. Fujitani, *J. Electrochem. Soc.* 154 (2007) A253-257.
27. J.W. Fergus, *J. Power Sources* 195 (2010) 939-954.